Importance of charge capture in interphase regions during readout of charge-coupled devices

Journal of Astronomical Telescopes, Instruments, and Systems

AstronomicalTelescopes.SPIEDigitalLibrary.org

Importance of charge capture in interphase regions during readout of charge-coupled devices

Jesper Skottfelt
David J. Hall
Ben Dryer
Nathan Bush
Jason P. D. Gow
Andrew D. Holland

SPIE.

Jesper Skottfelt, David J. Hall, Ben Dryer, Nathan Bush, Jason P. D. Gow, Andrew D. Holland, "Importance of charge capture in interphase regions during readout of charge-coupled devices," *J. Astron. Telesc. Instrum. Syst.* **4**(1), 018005 (2018), doi: 10.1117/1.JATIS.4.1.018005.

Importance of charge capture in interphase regions during readout of charge-coupled devices

Jesper Skottfelt,* David J. Hall, Ben Dryer, Nathan Bush, Jason P. D. Gow,† and Andrew D. Holland
Open University, Centre for Electronic Imaging, Milton Keynes, United Kingdom

Abstract. The current understanding of charge transfer dynamics in charge-coupled devices (CCDs) is that charge is moved so quickly from one phase to the next in a clocking sequence and with a density so low that trapping of charge in the interphase regions is negligible. However, simulation capabilities developed at the Centre for Electronic Imaging, which includes direct input of electron density simulations, have made it possible to investigate this assumption further. As part of the radiation testing campaign of the Euclid CCD273 devices, data have been obtained using the trap pumping method, a method that can be used to identify and characterize single defects within CCDs. Combining these data with simulations, we find that trapping during the transfer of charge among phases is indeed necessary to explain the results of the data analysis. This result could influence not only trap pumping theory and how trap pumping should be performed but also how a radiation-damaged CCD is readout in the most optimal way. [DOI: 10.1117/1.JATIS.4.1.018005]

Keywords: charge-coupled devices; radiation; simulations; image reconstruction.

Paper 17088 received Nov. 1, 2017; accepted for publication Mar. 9, 2018; published online Mar. 28, 2018.

1 Introduction

With the ever-increasing demand for higher photometric and spatial precision in data coming from space-based observatories, the ability to identify and characterize radiation-induced defects in detectors is of high importance. Defects are intrinsic in a silicon lattice, even in detectors of a very high quality, and new defects can be created by highly energetic particles, mainly from the Sun, that knock out atoms in the silicon lattice of the charge-coupled device (CCD). These defects are able to trap electrons during the readout phase of the CCD and release them at a later point in time, which effectively smears the image and, thereby, negatively affects the image quality. To be able to correct for this smearing, a high level of knowledge about the trap density and other physical properties is needed.

While methods such as first pixel response and extended pixel edge response[1] are only able to give information about average properties of the traps in the CCD, the trap pumping technique[2–7] is able to probe the individual traps. Trap pumping works by clocking charge back and forth among the pixels such that each trap creates a dipole for which the intensity depends on how close the emission time constant is to the clocking time. This means that information about the emission time constant, energy level, capture and emission cross sections, subpixel, and even subphase positions for the single traps can be extracted and a much better constraint on the trap density can be made.

The purpose of the VISible imager instrument (VIS)[8] on board Euclid,[9] the second medium-class mission in the European Space Agency's Cosmic Vision program, is to deliver high-resolution shape measurements of galaxies down to very faint limits ($R \sim 25$ at 10σ) in a large part of the sky. The measurement can then be used to infer the distribution of dark matter in the Universe. However, for this to be possible, it is important that the radiation-induced traps which accumulate in the detectors over the mission lifetime can be characterized and corrected for a high precision. For that purpose, trap pumping will be employed as part of the in-orbit calibration routines for the VIS instrument.[8] Trap pumping is, therefore, also a part of the radiation testing campaign, performed at the Centre for Electronic Imaging (CEI), of the CCD273 detectors[10] that will be used for the VIS instrument.

In a three-phase device with even-sized phases, as described in Sec. 2.1, the trap pumping dynamics can usually be worked out using symmetry considerations; however, for a four-phase device with uneven phase widths, such as the CCD273, this analysis can be more complicated. We have, therefore, used the CEI CCD Charge Transfer Model (C3TM) described in Ref. 11 (previously named OUMC) to simulate different trap pumping schemes.

In the preliminary testing of the CCD273 devices, interphase trapping was not observed, and following discussions with relevant experts in the field, the assumption has been that the transfer of charge among phases is sufficiently quick and over sufficient distance that the combined density/timing prevents trapping in the interphase regions. Combining the C3TM simulations with trap pumping data from a preirradiated CCD273 device, we are able to do further investigations into this assumption.

2 Trap Pumping Schemes

The trap pumping technique can be used for a variety of purposes, and the specific scheme used will depend on the desired output (cf. pocket pumping,[1] trap pumping for trap location and efficiency,[2,12,13] and trap pumping for trap emission time constants[3,5]) and the device used. We present several schemes that can be used depending on the device geometry. The main aim in these schemes is to determine the density and

*Address all correspondence to: Jesper Skottfelt, E-mail: jesper.skottfelt@open.ac.uk

†Present Address: University College London, Mullard Space Science Laboratory, Dorking, United Kingdom

2329-4124/2018/$25.00 © 2018 SPIE

properties of the traps toward the purpose of the correction of radiation damage effects in image postprocessing.

The theory behind the trap pumping technique is based on Shockley–Read–Hall (SRH) theory.[14,15] This states that trap release is governed by Poisson statistics, which imply a probability density function of the form $(1/\tau_e) \cdot \exp(-t/\tau_e)$, where τ_e is the emission time constant. The probability of release after an elapsed time t_δ is the integral of the function

$$P(t_\delta) = 1 - \exp\left(\frac{-t_\delta}{\tau_e}\right), \tag{1}$$

and the probability of release within a time interval $[t_1, t_2]$ is the difference of the two cumulative probabilities

$$P(t_2) - P(t_1) = \exp\left(\frac{-t_1}{\tau_e}\right) - \exp\left(\frac{-t_2}{\tau_e}\right). \tag{2}$$

2.1 *Three-Phase Device*

Trap pumping in a three-phase device is usually done by clocking the charge from phases 1-2-3-1′-3-2-1, where 1′ indicates phase 1 in the next pixel. The time the charge spends under each phase, the phase time ($t_{\rm ph}$), is the same for all the steps. From symmetry considerations and Eq. (2), it can be shown that a trap under phase 2 or 3 that captures an electron will release it into the adjacent charge cloud if the emission time constant (τ_e) of the trap is close to $t_{\rm ph}$, as shown in Fig. 1. This creates a dipole that can be amplified to be distinguishable from shot noise and readout noise (see Fig. 2) by repeating the clocking cycle a suitable number of times.

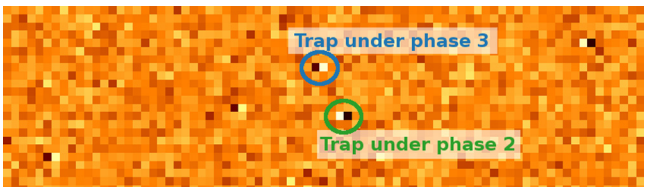

Fig. 2 Example of dipoles from trap pumped data. The direction of the dipoles reveals under which phase the trap is located.

By pumping with a range of $t_{\rm ph}$ values, it is possible to determine the emission time constant τ_e for the trap by fitting the dipole intensity curve, as shown in Fig. 3, with

$$I_{12} = N \cdot P_c \cdot \left[\exp\left(\frac{-t_{\rm ph}}{\tau_e}\right) - \exp\left(\frac{-2t_{\rm ph}}{\tau_e}\right)\right], \tag{3}$$

where N is the number of cycles and P_c is analog to the probability of capture (see also Sec. 2.1.2). The second part of the equation is taken directly from Eq. (2) using $t_1 = t_{\rm ph}$ and $t_2 = 2t_{\rm ph}$, and the subscript for I_{ij}, therefore, relates to the multiple of $t_{\rm ph}$ to be used. If the whole process is done at multiple temperatures, even more information about the trap, such as the energy level and emission cross section, can be retrieved.

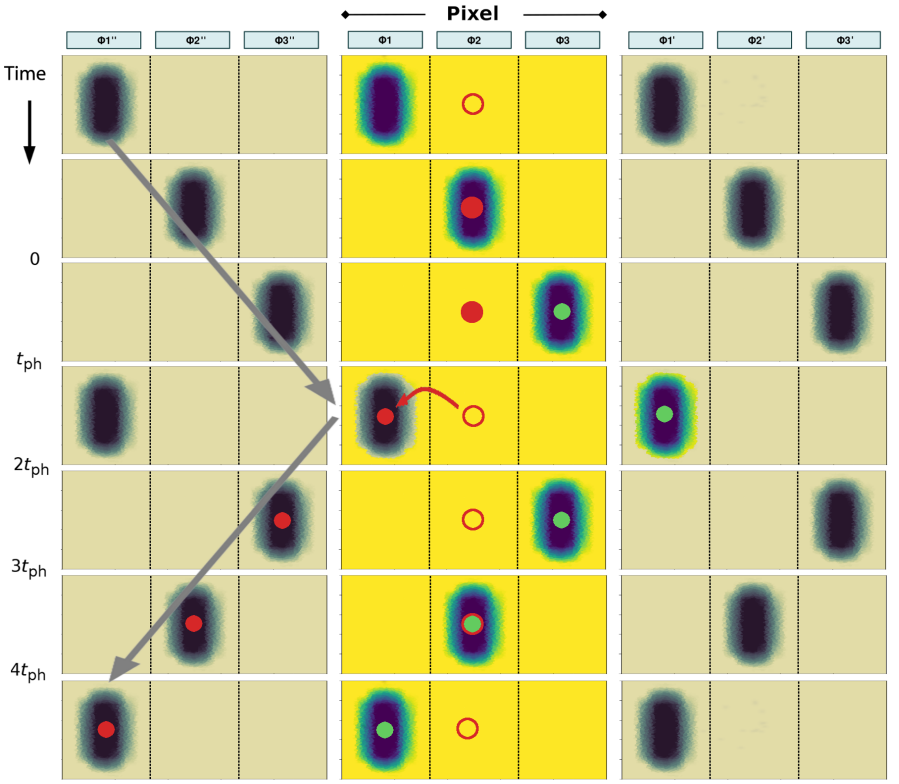

Fig. 1 Pumping from phases 1, 2, 3, 1′, 3, 2 and back to 1 (as indicated by the large gray arrow), where 1′ denotes the first phase in the next pixel. A trap under phase 2 can capture an electron, and if the emission of the electron happens between $t_{\rm ph}$ and $2t_{\rm ph}$, then the electron will be deposited in the adjacent charge packet. For simplicity, this figure does not show the transition steps where charge moves from one phase to the next.

2.1.1 *Position of trap in pixel*

A trap under phase 2 will move charge in the opposite direction of a trap under phase 3, so the polarity of the resulting dipole will also be opposite and this, thus, reveals under which of the two phases the trap is. A trap under phase 1 will in this situation be filled with charge from two charge packets, and a dipole will never form. To detect traps under phase 1, the pumping cycle, therefore, needs to be started under phase 2 or 3.

C3TM[11] is a Monte Carlo model that simulates the physical processes taking place when transferring the signal through a radiation-damaged CCD. The software is based on SRH theory and is made to mimic the physical properties in the CCD as closely as possible. The code runs on a single electrode level and takes three-dimensional trap position, potential structure of the pixel, and device specific simulations of electron density as a direct input, thereby avoiding the need to make any analytical assumptions about the size and density of the charge cloud.

With C3TM, it is, therefore, possible to make a map of the dipoles produced by traps depending on their position in the pixel. This is done by putting traps with a known τ_e value at a range of subpixel positions in a single line of pixels such that the first trap is placed in pixel 5 and at subpixel position 0.005, i.e., position 5.005, the next trap at 10.015, the next at 15.025, etc. This means that 99 traps, all with the same τ_e value, will have subpixels positions spread evenly over the pixel. A trap pumping scheme is then simulated for this line for a range of t_{ph} values and, thus, creating a dipole curve for each trap similar to the curve shown in the lower panel of Fig. 3.

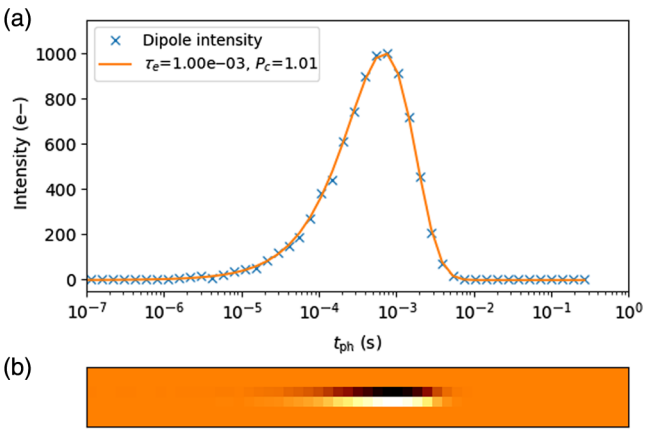

Fig. 3 (b) Simulation using C3TM of a trap pumped over a range of t_{ph} values, producing dipoles of different intensities. (a) The intensities of the bright part of the dipole panel below are plotted on a matching *x*-axis (crosses) and fitted with Eq. (3) (fit shown as solid line), thereby obtaining τ_e and P_c for the given trap.

For a three-phase device using the standard clocking scheme, the map of dipoles is shown in Fig. 4. As expected, this shows that a trap under phase 2 will pump electrons into the charge cloud in the pixel to the left, and a trap under phase 3 will pump to the pixel to the right, whereas traps under phase 1 do not pump.

2.1.2 *Probability of capture and the P_c quantity*

In SRH theory, the probability of capture after a certain time is the same as Eq. (1) but using a capture time constant (τ_c) instead of an emission time constant (τ_e).

The definition of τ_c is

$$\tau_c = \frac{1}{\sigma n v_{\mathrm{th}}}, \tag{4}$$

where σ is the capture cross section, n is the electron density, and v_{th} is the thermal velocity. While σ and v_{th} are constants, n depends on a number of variables, such as pixel geometry, position of the trap in the pixel, signal size, and clocking scheme. To get the best physical representation of n, the C3TM software uses device specific simulations of the electron density as a direct input. A more detailed description of this can be found in Ref. 11, but Fig. 1 gives an indication of the size of the charge cloud at 100,000 e^-. Figures later in the paper will give an idea of how the size of the charge cloud changes with signal level.

The P_c quantity used in Eq. (3) is best thought of as the efficiency of capture during the trap pumping process. It is, therefore, related to the capture probability as it is described in SRH theory, but the two quantities will not scale linearly as the term includes an element of the probability of the trap being empty and thus being able to capture. Also, while the capture probability in SRH theory only relates to a single trap, then P_c could describe a combination of multiple traps in the same pixel, and if these were to pump in the same direction, it could generate values of $P_c \gg 1$.

2.2 *Four-Phase Device*

The four-phase structure of the CCD273's parallel (or image) register means that there are several possible trap pumping clocking schemes to consider. An obvious choice would be to simply add the extra phase and pump 1-2-3-4-1′-4-3-2-1 as presented in Ref. 5. The extra phase step means that depending on under which phase, and even where in the phase, the traps are positioned, and the dipole intensity needs to be fit with either Eq. (3) or one of the two following equations:

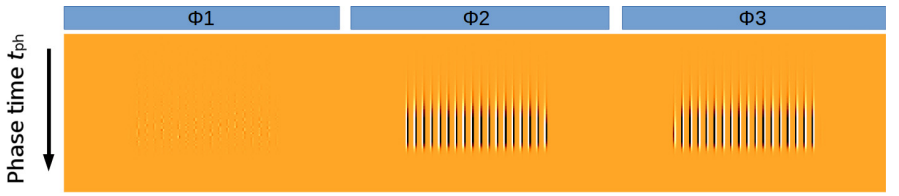

Fig. 4 Dipole map of a three-phase device using the standard 1-2-3-1′-3-2-1 clocking scheme, showing that traps under phases 2 and 3 will pump in different directions and that traps under phase 1 will not pump. A signal level of 100,000 e^- is used, and the extend of where trap pumping occurs under phase 2 and 3, therefore, gives the idea of the width of the charge cloud.

$$I_{23} = N \cdot P_c \cdot \left[\exp\left(\frac{-2t_{\mathrm{ph}}}{\tau_e}\right) - \exp\left(\frac{-3t_{\mathrm{ph}}}{\tau_e}\right)\right], \quad (5)$$

$$I_{14} = N \cdot P_c \cdot \left[\exp\left(\frac{-t_{\mathrm{ph}}}{\tau_e}\right) - \exp\left(\frac{-4t_{\mathrm{ph}}}{\tau_e}\right)\right]. \quad (6)$$

This means that three different τ_e values could be found for the same trap. By starting at multiple starting points for the trap pumping cycle, it would be possible to get information relating not only to which phase the trap is under but also where in the phase. However, with the 4-2-4-2-μm widths of the phases in the CCD273, this information becomes very difficult to disentangle. An example of this is shown in Fig. 5, where C3TM is used to simulate how the dipole of a trap located at various points in a pixel would look.

In the normal readout mode for the Euclid VIS instrument, the parallel register is clocked with overlapping phases. To mimic this more closely, a trap pumping clocking scheme with overlapping phases could, therefore, also be used, such as 12-23-34-41′-1′2′-41′-34-23-12. A simulation of this pumping scheme is shown in Fig. 6 for two different signal levels, 100,000 e^- and 1000 e^-.

For the 100,000 e^- level, it is seen that at certain places the traps will continue to pump for all t_{ph} values over a certain threshold. This comes from the uneven sizes of the phases, which mean that when the signal is moved from one phase to the next, there is a chance that the neighboring charge cloud will always be closer to that particular trap, unless the charge is actually in the phase itself. This means that as long as the t_{ph} value is longer than the capture time constant τ_c, then that particular trap will always pump, and we, therefore, refer to them as "always pump" traps. The resulting dipole can be fit with

$$I_{\mathrm{ap}} = N \cdot P_c \cdot \left[1 - \exp\left(\frac{-k \cdot t_{\mathrm{ph}}}{\tau_e}\right)\right], \quad (7)$$

where k depends on the pumping scheme and the position of the trap in the pixel. Figure 6 shows that there is a large difference between which types of dipoles we see at different signal levels, and it would, therefore, be difficult to figure out which equation to use to find the right τ_e value, if this pumping scheme was used.

Furthermore, a three-level clocking scheme[16] is used in normal operations of the Euclid VIS instrument; however, we found that trap pumping with a three-level trap pumping scheme only increased the complexity and, thus, makes it even harder to disentangle the single traps.

2.3 *Pseudo-Three-Phase Clocking*

Another option for a four-phase device is to mimic a three-phase device by coupling two phases together, i.e., 12-3-4-1′2′-4-3-12, thus getting a pseudo-three-phase clocking scheme. Simulations of this scheme are shown in Fig. 7 for four signal levels ranging from 100,000 e^- to 100 e^-, and these show that this scheme should only contain I_{12} dipoles and always pump dipoles. It was, therefore, decided to test if pseudo-three-phase clocking could be used for the Euclid in-orbit calibration routines, and the data in this paper are, therefore, based on this clocking scheme. To map the full pixel and to be able to disentangle

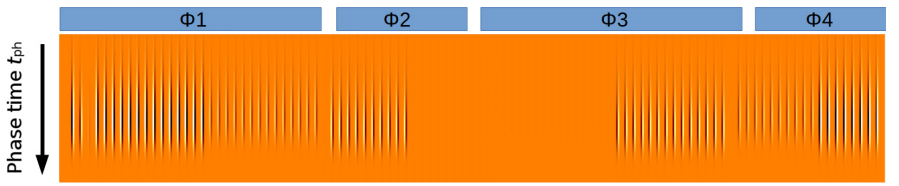

Fig. 5 Simulation of a four-phase nonoverlapping trap pumping scheme (1-2-3-4-1′-4-3-2-1) at 100,000 e^-, showing that dipole intensities need to be fitted with three different equations [Eqs. (3), (5), and (6)] depending on the position of the trap in the pixel.

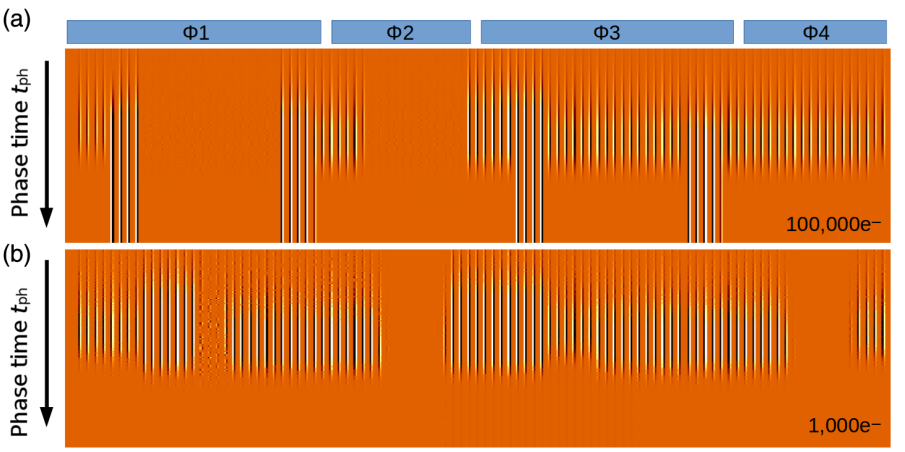

Fig. 6 Simulation of a four-phase overlapping trap pumping scheme (12-23-34-41′-1′2′-41′-34-23-12) at two signal levels, (a) 100,000 e^- and (b) 1000 e^-, showing that dipole intensities need to be fit with four different equations [Eqs. (3), (5)–(7)], depending on the position of the trap in the pixel.

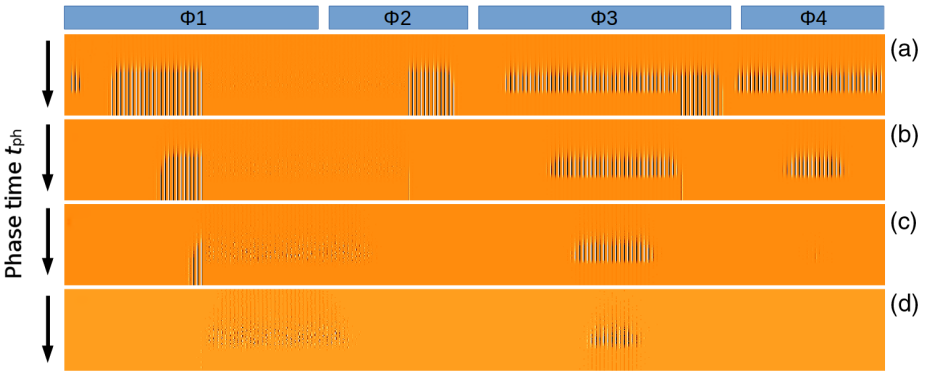

Fig. 7 Simulation of the pseudo-three-phase clocking scheme (12-3-4-1′2′-4-3-12) at four signal levels: (a) 100,000 e^-, (b) 10,000 e^-, (c) 1000 e^-, and (d) 100 e^-.

the traps, three identical trap pumping schemes are needed, starting at phases 12 (12-3-4-scheme), 23 (23-4-1-scheme), and 34 (34-1-2-scheme).

2.4 *Subpixel Clocking*

In parallel with this work, the subpixel clocking scheme was developed for the P- versus N-channel CCD irradiation study performed at the CEI.[17] This clocking scheme only moves the charge between three of the four phases in the device, such that pumping will only occur in the outer half of the end phases. This means that it, among other things, is possible to get much better positional information about the traps, even down to subphase precision.

Based on the results from the work presented in this paper, it was decided that the subpixel clocking scheme should be used for the Euclid testing campaign instead. For a more thorough description of the subpixel clocking scheme and the results, it gives on preirradiated CCD273 devices, see Ref. 18.

3 Experimental Data and Initial Analysis

The data for this analysis have been obtained from the image region of a preirradiated CCD273-EM1A device using the pseudo-three-phase clocking scheme. The CCD and its headboard are mounted inside a vacuum chamber that allows the device to be cooled to cryogenic temperatures using a CryoTiger refrigeration system. Two LEDs behind diffusers are mounted inside the vacuum chamber to deliver flat-field illumination, and before the data are analyzed, any pixel-to-pixel nonuniformities or gradients in the flat-field signal are calibrated out. A similar setup is used in Ref. 19, where it is also described in more detail.

Each scheme is run at a number of signal levels, ranging from 1600 e^- to 25,000 e^-, and three different temperatures (149, 153, and 157 K), and a range of t_{ph} values between 4 μs and 15 ms. In the following, the data taken at 153 K and at a signal level of 1600 e^- are used, but these are representative of the rest of the dataset.

Using an automated dipole detection, algorithm traps over the whole chip are detected and characterized. The algorithm fits each dipole intensity curve with both Eq. (3) (I_{12}) and Eq. (7) (I_{ap}) and then uses a χ^2 value to determine which τ_e value to use. Also, fit is a combination of the I_{12} and I_{ap} to fit multiple traps in the same pixel and a constant function, which is used to get rid of false dipoles. The algorithm outputs the pixel and phase position of the trap, the latter determined by the direction of the dipole, and the best-fit values for τ_e and P_c.

Figure 8 shows the I_{12} dipoles detected for each of the three schemes. The left-hand side plots are histograms of the τ_e values, whereas the right-hand side plots show the τ_e value versus the P_c value for each detected trap. While $P_c > 1$ values in theory only should be possible if multiple traps in the same pixel were pumping in the same direction as described in Sec. 2.1.2, then the P_c values up to ~1.2 are more likely attributed to the combined uncertainty of the dipole intensities and the fit to the dipole intensity curve.

Common for the histograms for all three schemes are that they have six peaks, or rather three double peaks, as each pair of τ_e peaks are almost a multiple of two apart. This suggests that for each double peak only one of them is a "real" species and the other one is an alias. As it is the rightmost peak for each double peak, that is closest to the expected capture probability, $P_c = 1$, this suggests that the leftmost peaks are aliases. Double peaks similar to what is found here have been seen in previous trap pumping data studies,[20] but no conclusive explanation has been found so far.

Another curious thing is that a number of traps have capture efficiency $P_c \gg 1$, especially for the 23-4-1 and 34-1-2 schemes, and that these seem to be consistent with the small third peak in between the two main peaks. As mentioned above, then $P_c \gg 1$ values are possible if multiple traps in the same pixel are pumping in the same direction, but we do not expect this to happen so frequently considering the low signal level and that unirradiated devices are used.

4 Investigation of Aliased Peaks

From the simulation in Fig. 7, it is possible to infer under which phase the trap is positioned simply by determining the orientation of the dipole, as described in Sec. 2.1. The 12-3-4-scheme should, therefore, pump traps under phase 3 with dipoles in one direction and traps under phase 4 in the other direction. Similarly, for the 23-4-1-scheme, it will pump phase 4 traps in one direction and phase 1 traps in the other. This means that traps under phase 4 should be detected by both the 12-3-4-scheme and the 23-4-1-scheme and, thus, make it possible to compare the τ_e value for the same trap from two different schemes.

Figure 9 shows the comparison of traps under the same phase in terms of τ_e and P_c values as found by two different schemes. The traps found with the same τ_e value (within 20%) in the two schemes are all pumping with the expected P_c value of about 1.

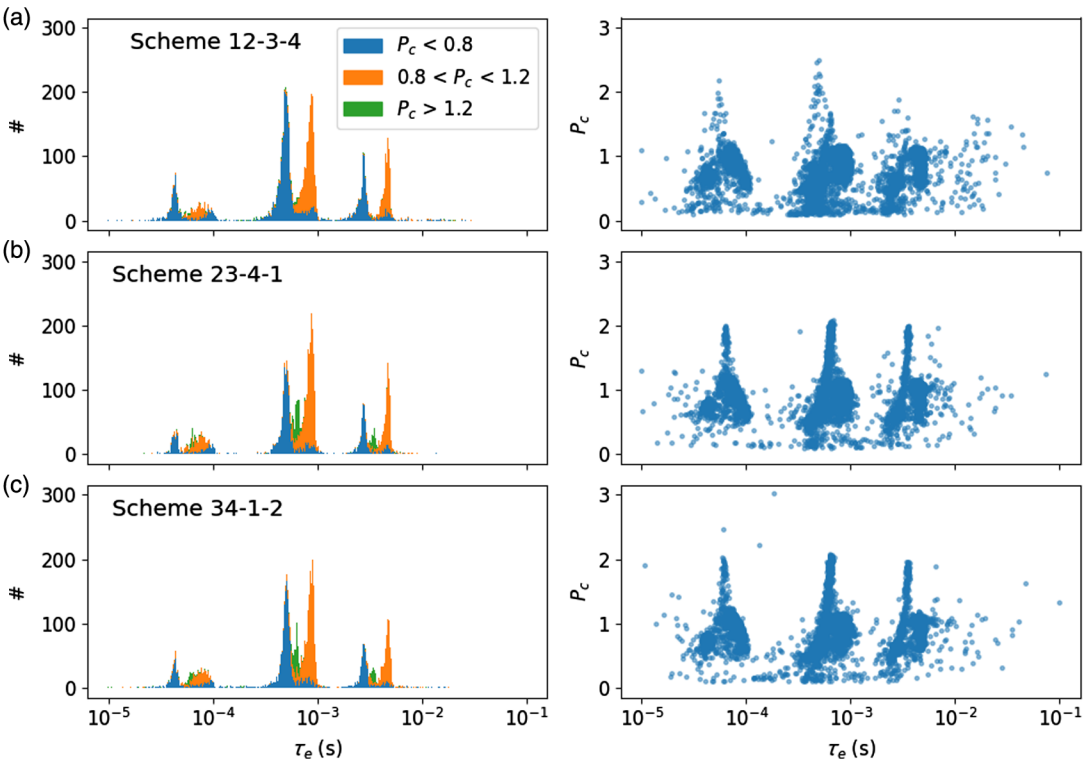

Fig. 8 I_{12} dipoles from trap pumping data made for 1600 e^- at 153 K. All plots are made from pseudo-three-phase clocking data: (a) 12-3-4-scheme, (b) 23-4-1-scheme, and (c) 34-1-2-scheme. The left-hand side plots are stacked histograms of the τ_e values, separated into the dipoles where $P_c < 0.8$ (blue), $0.8 < P_c < 1.2$ (orange), and $P_c > 1.2$ (green). The right-hand side plots show the τ_e value versus the P_c value for each detected trap.

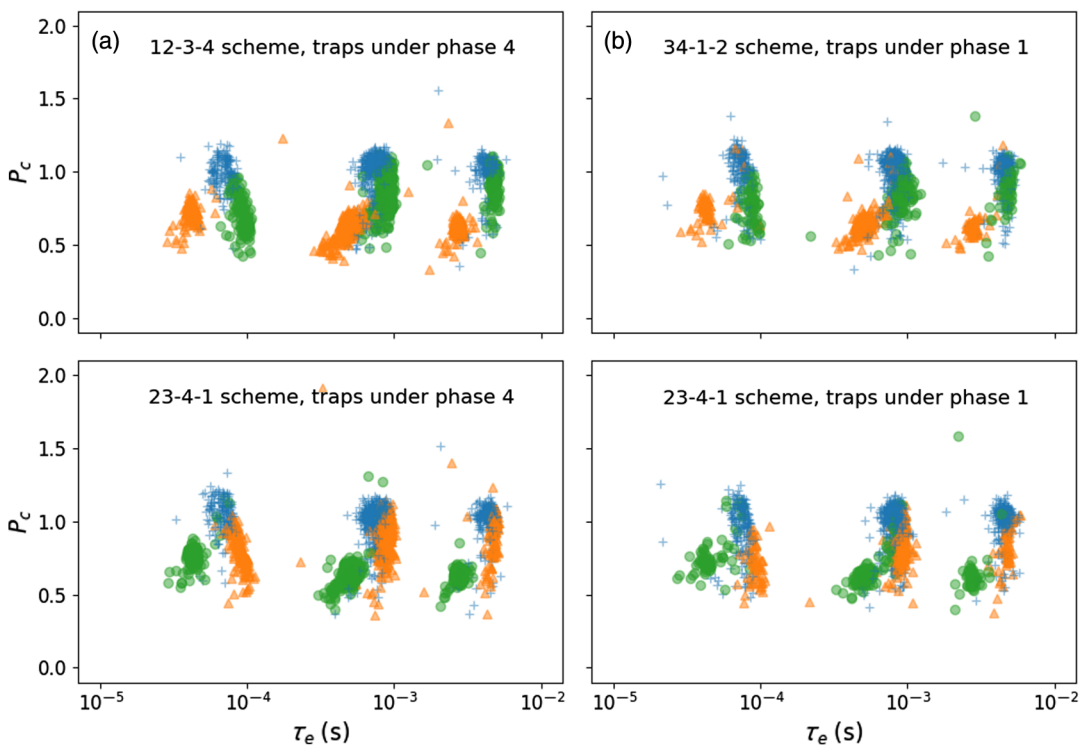

Fig. 9 (a) Comparison of I_{12} dipoles under phase 4 for the 12-3-4-scheme (top) and 23-4-1-scheme (bottom). The blue crosses show the traps where the same τ_e value within 20% was found in both schemes. The orange triangles show where the τ_e value found in the 23-4-1-scheme is more than 20% larger than the value found in the 12-3-4-scheme, and vice versa for the green circles. (b) Same as left side, but for traps under phase 1, with 34-1-2-scheme (top) and 23-4-1-scheme (bottom).

Traps where the difference in the τ_e value is more than 20% seem to be clustered either at the expected τ_e and P_c values or at about $0.6 \cdot \tau_e$ and $0.6 \cdot P_c$.

Empirically, it can be shown that if a distribution of intensities made with I_{23} using a set of emission time constants and capture efficiency, denoted $\tau_{e,23}$ and $P_{c,23}$ respectively, is fit with I_{12}, then values of $\tau_{e,12} \approx 0.6 \cdot \tau_{e,23}$ and $P_{c,12} \approx 0.6 \cdot P_{c,23}$ are found. Similarly, if a distribution of intensities made with I_{14} using $\tau_{e,14}$ and $P_{c,14}$ is fit with I_{12}, then values of $\tau_{e,12} \approx 0.7 \cdot \tau_{e,14}$ and $P_{c,12} \approx 1.8 \cdot P_{c,14}$ will be found. We, therefore, believe that the rightmost peak (shown with the orange circles in top right plot of Fig. 10) of each double peak is I_{12} dipoles, whereas the leftmost peak (green circles) should be fit with I_{23} instead. The dipoles with $P_c > 1$ (red circles) should be fit with I_{14} instead. If the results from Fig. 9 are used to determine which equation should be used, then we are able to produce a

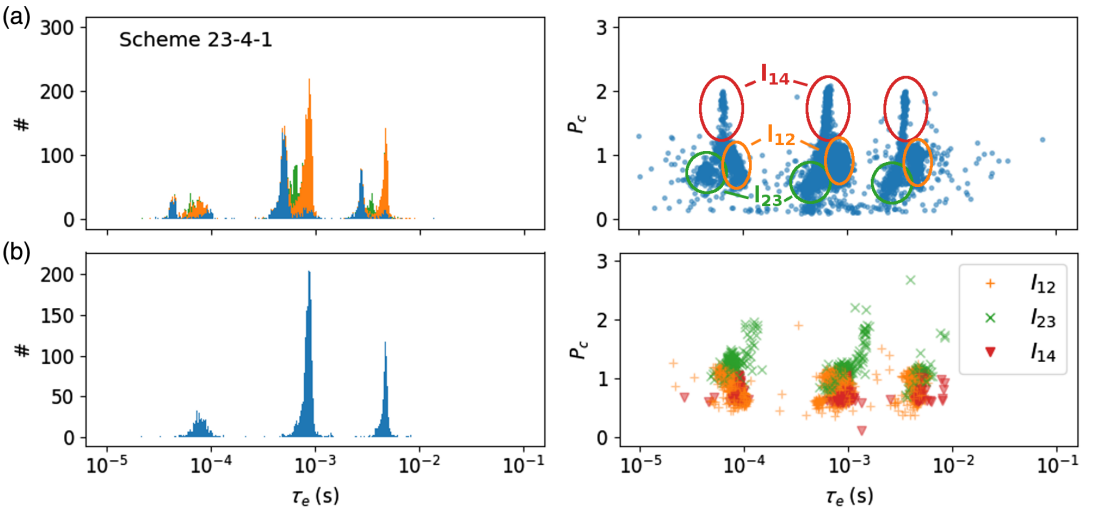

Fig. 10 (a) Cut-out of the 23-4-1-scheme (middle plots in Fig. 8) with indications of which equations to use for fitting dipoles at different positions in the τ_e versus P_c plot. (b) Using results from Fig. 9 to determine which fit to use for τ_e and P_c shows that a single peak for each of the three species can be obtained.

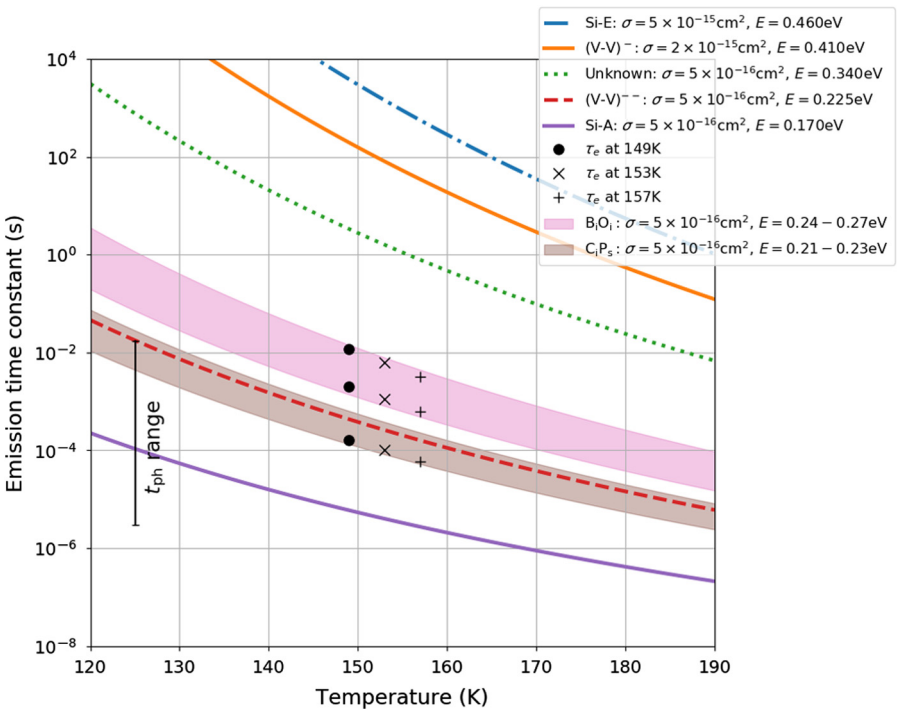

Fig. 11 Emission time constants of five well-known defects [Si-E, $(V - V)^-$, "unknown," $(V - V)^{--}$, Si-A] as a function of temperature. The three peaks from the corrected pseudo-three-phase data are shown as dots, x'es, and plusses for 149, 153, and 157 K, respectively. The ranges for the boron-interstitial-oxygen-interstitial (B_iO_i) and the carbon-interstitial-phosphorus-substitution (C_iP_s) are also shown. The vertical bar at 125 K shows the range of t_{ph} values used in these trap pumping tests.

histogram (bottom left plot of Fig. 10) with only one peak per species.

By fitting a Gaussian distribution to each of the peaks in the corrected plot, the τ_e value for each of the three species can be obtained. This has been done for all three temperatures, and in Fig. 11, the τ_e-peak values are plotted in a τ_e versus temperature plot with "well-known" species, i.e., the species that are usually found in irradiated devices.[5] The plot shows that the three peaks follow the same trend as the known species, and the energy levels of the new species are estimated to be 0.21, 0.245, and 0.265 eV. These energy levels are consistent with phosphorus-carbon and boron-oxygen impurities, which in Ref. 21 are quoted to have energies in the ranges of 0.21 to 0.23 eV and 0.24 to 0.27 eV, respectively. Boron and phosphorus are used as dopants in CCDs, and carbon and oxygen are naturally occurring impurities in the silicon wafers from which the CCD is manufactured. It should be noted that these energy levels assume a capture cross section of 5×10^{-16} cm^2, and to get better precision of these two values, the data need to be obtained at a broader range of temperatures.

That none of the well-known species are found in these data are not surprising, as the data are from an unirradiated device. However, after irradiation, we expect the well-known species to become much more abundant and most likely render the species found here negligible. The energy levels found here match very well with the energy levels found in the subpixel scheme described in Sec. 2.4, which has now been chosen for the Euclid in-orbit calibrations based on the work in this paper.[18]

5 Discussion

It is normally assumed that signal charge moves so fast from one electrode to the next during transfer, and with a low density over the interphase spacing, that no charge will be trapped in this transition, i.e., trapping only occurs when the charge sits under the phase during the t_{ph} time. This assumption is based on the width of the barrier among the phases, and the speed of an electron moving among changing potentials, and it is only with our more advanced models that this can be fully tested.

An analysis of the movement of the charge cloud during the trap pumping sequence with the new simulations, shown in Fig. 12, shows that if trapping is happening when the charge is moved from one phase step to the next, this would explain the origin of the I_{23} and I_{14} dipoles.

A simulation of the pseudo-three-phase scheme on a two-dimensional pixel array was performed using C3TM. Traps with energy levels of [0.17, 0.21, 0.24, 0.265, 0.34] eV were inserted in random pixels to reach a trap density for each energy level of 5×10^2 traps cm^{-3}, and a signal level of 1600 e$^-$ was applied. When running the simulation without any transition phase (Fig. 13 upper panel) the τ_e versus P_c plot does not match the one seen in Fig. 8; however, when a 100-ns transition phase is added (Fig. 13 lower panel), they look much more alike.

Figure 14 is a simulation of the 12-3-4-scheme, but with a 100-ns transition step in between each phase step. This shows a much more complicated dipole map than Fig. 7 where no transition step is included, and it seems to confirm the positions of the I_{23} and I_{14} dipoles. It also shows that the position of the different dipole types are much more dependent on the signal level, than if there is no transition step, and this might make it much harder to disentangle the positions of the traps.

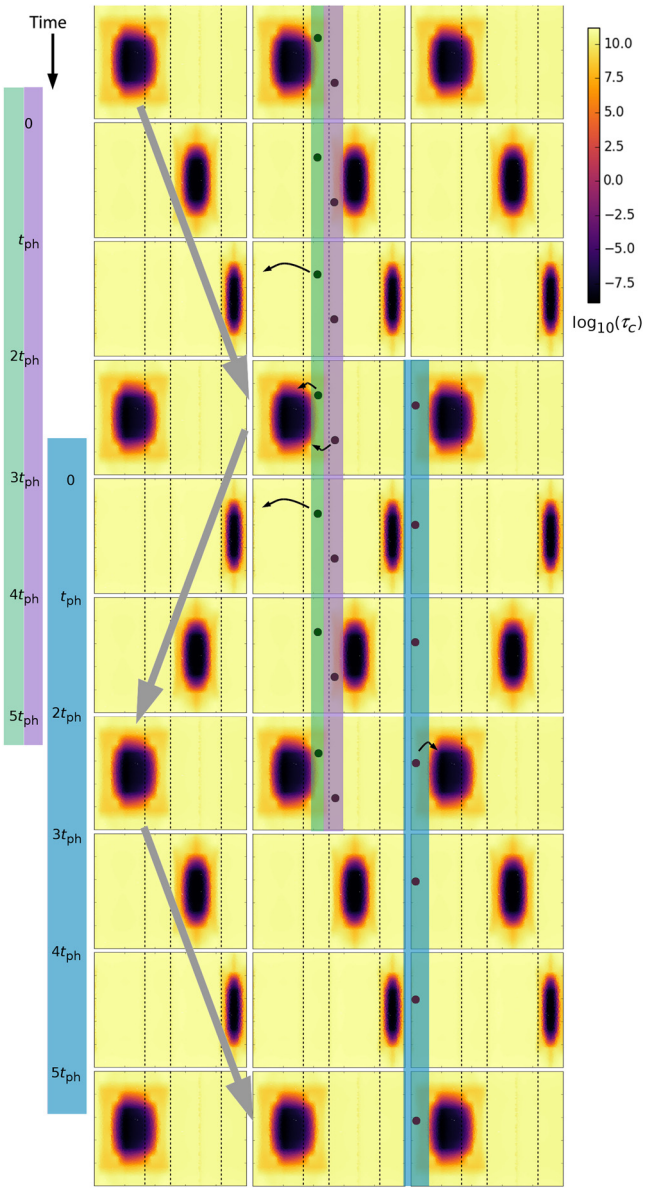

Fig. 12 Analysis of the movement of the charge cloud during a trap pumping sequence, where the large gray arrows show the movement of a single charge cloud during a single cycle. The black dots show the position of a trap, and the small black arrows shown when a trap would emit to a neighboring charge from which it has been captured if trapping can happen when charge is moved from one phase step to the next. The purple and blue (green) areas show the position in the pixel of traps creating I_{23} (I_{14}) dipoles.

Figure 15 shows simulations of the 12-3-4-scheme at a range of different transition-step times. This shows that even with a 1-ns transition phase the I_{23} and I_{14} dipoles are visible, although very faint, and that the intensity of these dipoles rises with longer transition times. By doing a more thorough comparison of simulations and lab data, it might be possible to further constrain the length of the transition phase.

Interphase trapping seems to have a profound effect on trap pumping theory and it emphasizes the importance of being able to simulate the dynamics of the chosen trap pumping scheme to a very high precision. However, it could also affect how a radiation-damaged CCD is readout in the most optimal way. In the

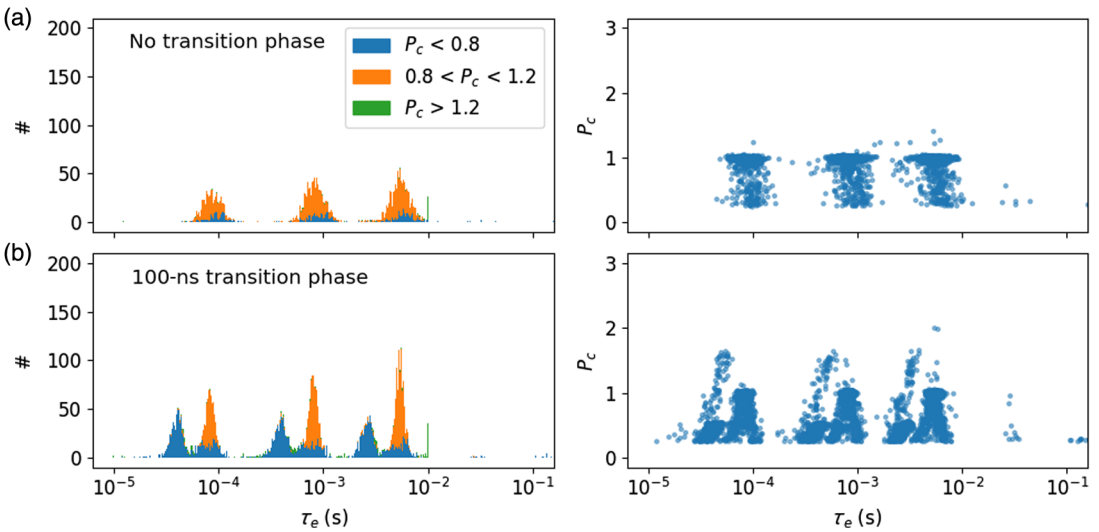

Fig. 13 Simulation of the pseudo-three-phase scheme using C3TM for 1600 e^- at 153 K, i.e., the same parameters as in Fig. 8. Traps with five different energy levels (see details in text) are created at random positions in an array, and the trap pumping is simulated (a) without any transition phase and (b) with a 100-ns transition phase.

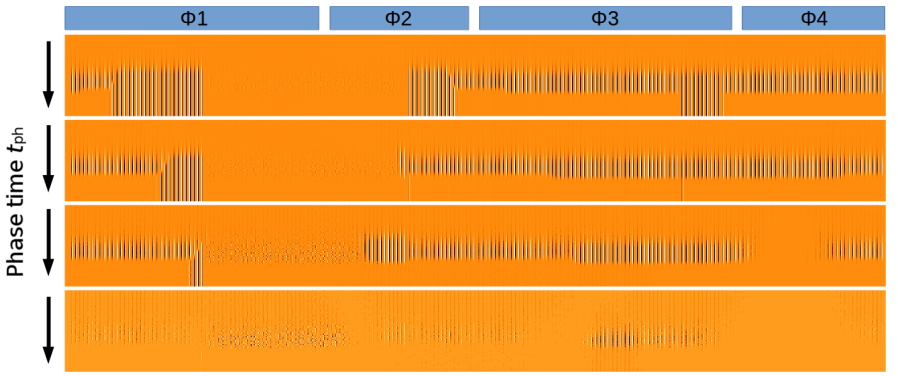

Fig. 14 Same as Fig. 7, but with a 100-ns transition among each phase step.

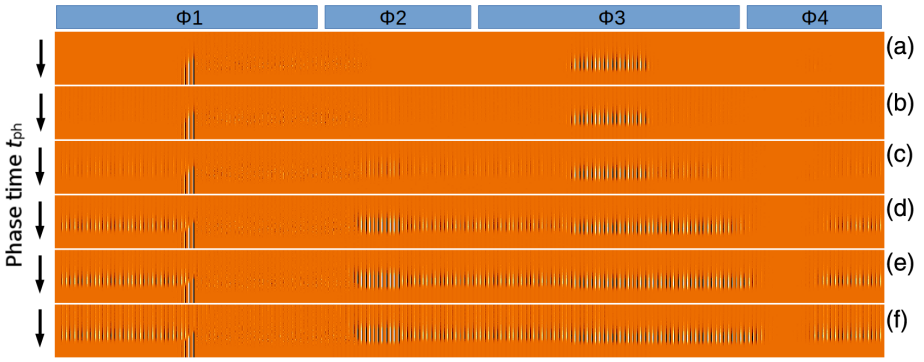

Fig. 15 Simulation of the 12-3-4-scheme at a signal level of 1000 e^-, for a transition phase times of (a) 0 s, (b) 1 ns, (c) 10 ns, (d) 100 ns, (e) 1 μs, and (f) 10 μs.

case of the Euclid CCD273, the baselined readout scheme for the parallel register is to always clock with overlapping phases (12-23-34-41′-1′2′-2′3′...). This means that traps located among phases will be encountered by the signal charge at each stage of the transfer in the Euclid parallel readout, with the charge held under at least two neighboring phases at all times. If instead a nonoverlapping readout scheme (1-2-3-4-1′-2′-...) had been chosen, interphase trapping could potentially occur at each transition step, resulting in worse than anticipated charge transfer efficiency and changing the way in which one might choose to optimize the device readout.

6 Conclusion

The common assumption of charge transfer dynamics has been that the charge moves so fast between each step of the sequence, and with a low density over the interphase spacing, that no charge will be trapped in this transition. However, trap pumping data made as part of the CCD273 irradiation campaign for the Euclid mission do not match that assumption.

After a thorough analysis of the data, we find that the only explanation is indeed that interphase trapping must be happening. We are further able to identify from which parts of the pixel the interphase trapping is most likely to occur. These results are reproduced by simulations implemented with the CEI CCD Charge Transfer Model (C3TM), which also show that the data are consistent with having a short transition phase among each transfer. The length of the transition phase could be as low as a few ns, but a more thorough comparison of simulations and lab data will be completed in the future to constrain this.

As interphase trapping can occur not only when doing trap pumping, but also in a normal readout of the detector, this result can affect how a radiation-damaged CCD is readout in the most optimal way. It will not influence the normal parallel readout of the Euclid CCD273 device, as this is always clocked with overlapping electrodes, but based on this work another trap pumping scheme, the subpixel scheme, has been chosen for the Euclid in-orbit calibrations as detailed in Ref. 18.

References

1. J. R. Janesick, *Scientific Charge-Coupled Devices*, SPIE Press, Bellingham, Washington (2001).
2. N. J. Murray et al., "Mitigating radiation-induced charge transfer inefficiency in full-frame CCD applications by 'pumping' traps," *Proc. SPIE* **8453**, 845317 (2012).
3. D. J. Hall et al., "Determination of in situ trap properties in CCDs using a 'single-trap pumping' technique," *IEEE Trans. Nucl. Sci.* **61**, 1826–1833 (2014).
4. D. Wood et al., "Studying charge-trapping defects within the silicon lattice of a p-channel CCD using a single-trap 'pumping' technique," *J. Instrum.* **9**(12), C12028 (2014).
5. D. Hall et al., "Mapping radiation-induced defects in CCDS through space and time," *Proc. SPIE* **9915**, 99150I (2016).
6. D. J. Hall et al., "In situ trap properties in CCDs: the donor level of the silicon divacancy," *J. Instrum.* **12**, P01025 (2017).
7. D. Wood et al., "Evolution and impact of defects in a p-channel CCD after cryogenic proton-irradiation," *IEEE Trans. Nucl. Sci.* **64**, 2814–2821 (2017).
8. M. Cropper et al., "VIS: the visible imager for Euclid," *Proc. SPIE* **9904**, 99040Q (2016).
9. R. Laureijs et al., "Euclid definition study report," arXiv:1110.3193 (2011).
10. A. D. Short et al., "The Euclid VIS CCD detector design, development, and programme status," *Proc. SPIE* **9154**, 91540R (2014).
11. J. Skottfelt et al., "Comparing simulations and test data of a radiation damaged charge-coupled device for the Euclid mission," *J. Astron. Telesc. Instrum. Syst.* **3**(2), 028001 (2017).
12. R. Kohley, F. Raison, and J. M. Martin-Fleitas, "Gaia: operational aspects and tests of Gaia Flight Model CCDs," *Proc. SPIE* **7439**, 74390F (2009).
13. N. J. Mostek et al., "Charge trap identification for proton-irradiated p+ channel CCDs," *Proc. SPIE* **7742**, 774216 (2010).
14. W. Shockley and W. T. Read, "Statistics of the recombinations of holes and electrons," *Phys. Rev.* **87**, 835–842 (1952).
15. R. N. Hall, "Electron–hole recombination in germanium," *Phys. Rev.* **87**, 387–387 (1952).
16. N. J. Murray et al., "Multi-level parallel clocking of CCDs for: improving charge transfer efficiency, clearing persistence, clocked anti-blooming, and generating low-noise backgrounds for pumping," *Proc. SPIE* **8860**, 88600K (2013).
17. N. Bush et al., "A comparison of proton damage effects on P- and N-channel CCDs I: performance following cryogenic irradiation," (2018), in preparation.
18. J. Skottfelt et al., "Trap pumping schemes for the Euclid CCD273 detector: characterisation of electrodes and defects," *J. Instrum.* **12**(12), C12033 (2017).
19. J. P. D. Gow et al., "Assessment of proton radiation-induced charge transfer inefficiency in the CCD273 detector for the Euclid Dark Energy Mission," *Proc. SPIE* **8453**, 845316 (2012).
20. D. Wood et al., "A study of the double-acceptor level of the silicon divacancy in a proton irradiated n-channel CCD," *Proc. SPIE* **9915**, 99150J (2016).
21. P. Pichler, *Intrinsic Point Defects, Impurities, and Their Diffusion in Silicon*, Computational Microelectronics, Springer-Verlag, Wien, New York (2004).

Jesper Skottfelt is a research fellow at the Centre for Electronic Imaging (CEI), the Open University, United Kingdom. He did his PhD in astronomy at the Niels Bohr Institute, Copenhagen University, Denmark, where he worked on an EM-CCD instrument. He is working on several projects involving ground- and space-based imaging, including simulating charge transfer in radiation-damaged charge-coupled devices (CCDs) to provide input to the radiation damage correction efforts for future space missions.

David J. Hall is a lecturer of physical sciences at the Open University within the CEI. He studied physics at the University of Oxford before completing his PhD at the CEI. Over the last 11 years, he has specialized in research in radiation damage and radiation defects in silicon detectors, and radiation-induced background in space-borne detectors, working on many ESA and NASA missions, including Gaia, Euclid, Athena, SMILE, and WFIRST.

Ben Dryer is a postdoc at the CEI, Open University. He studied physics with industrial experience at the University of Bristol, followed by studying toward his PhD within the CEI. He is interested in the effects of radiation damage on space-borne silicon imaging sensors and is focused on how best to assess the damage effects for scientific operations through ground-based testing of CCDs and CMOS imaging sensors.

Nathan Bush is a research fellow at the CEI, Open University, United Kingdom. He studied physics with astrophysics at the University of Sussex before completing his PhD at the Open University, researching the impact of radiation damage on EM-CCD technology for large-scale space missions. His research at the Open University is focused on the optimization of EM-CCD sensors in the presence of particle-induced damage, the nature and behavior of defects within silicon devices, and the development of radiation hard imaging technologies.

Jason P. D. Gow is the PLATO detector scientist working at the University College London's Mullard Space Science Laboratory, previously having worked at the CEI as a research fellow. He was awarded his PhD from Brunel University for work on radiation damage mitigation for the detectors used in the C1XS instrument. He is interested in predicting, understanding, and mitigating the impact of radiation damage on CCD and CMOS imaging sensors for space applications.

Andrew D. Holland is a professor in electro-optics and head of the CEI, the Open University, United Kingdom. He is an expert in detector physics and has worked on the development of a number of successful space instruments. Working on a range of detector developments over the past two decades, he has a wealth of knowledge and experience advising on instrument-related issues, in particular radiation damage effects.